Investigating Cavity Quantum Electrodynamics-Enabled Endo/Exo-Selectivities in a Diels-Alder Reaction

Jialong Wang,[†] Braden M. Weight,[*,‡] and Pengfei Huo[*,†,¶]

†*Department of Chemistry, University of Rochester, Rochester, NY 14627, U.S.A.*
‡*Department of Physics and Astronomy, University of Rochester, Rochester, NY 14627, U.S.A.*
¶*The Institute of Optics, Hajim School of Engineering, University of Rochester, Rochester, NY 14627, U.S.A.*

E-mail: bweight@ur.rochester.edu; pengfei.huo@rochester.edu

Abstract

Coupling molecules to a quantized radiation field inside an optical cavity has shown great promise in modifying chemical reactivity. It was recently proposed that strong light-matter interactions are able to differentiate endo/exo products of a Diels-Alder reaction at the transition state. Using the recently developed parameterized quantum electrodynamic *ab initio* polariton chemistry approach along with time-dependent density functional theory, we theoretically confirm that the ground state selectivity of a Diels-Alder reaction can be fundamentally changed by strongly coupling to the cavity, generating preferential endo or exo isomers which are formed with equal probability for the same reaction outside the cavity. This provides an important and necessary benchmark with the high-level self-consistent QED coupled cluster approach. In addition, by computing the ground state difference density, we show that the cavity induces a redistribution of electron density from intramolecular π-bonding orbitals to intermolecular bonding orbitals, thus providing chemically relavent description of the cavity-induced changes to the ground state chemistry and thus changes to the molecular orbital theory inside the cavity. We extend this exploration to an arbitrary cavity polarization vector which leads to critical polarization angles that maximize the endo=/exo selectivity of the reaction. Finally, we decompose the energy contributions from the Hamiltonian and provide discussion relating to the dominent dipole self-energy effects on the ground state.

Introduction.

The Diels-Alder (DA) reaction, first elucidated in the previous century, stands as a cornerstone of organic synthesis. This cycloaddition reaction involves the formation of a conjugated diene and a dienophile, typically an alkene, culminating in a substituted cyclohexene system. DA reactions are one of most useful techniques for creating carbon-carbon bonds.[1,2] Furthermore, such reactions were fundamental in the creation of famous the Woodward-Hoffmann rules,[3] a set of principles governing the stereochemistry of organic reactions. Of particular note for common DA reactions are their capacity to result in either an "endo" or "exo" isomer during the formation of the transition state. This results in two distinct products. More specifically, if we consider the reaction between cyclopentadiene and acrylonitrile (see Fig. 1a), the resulting products under ambient conditions are known provide endo and exo in equal proportion (*i.e.*, no selectivity).

It was recently proposed that strong light-matter interactions are able to differentiate these products at the transition state via coupling the molecular system to the quantized photon field inside an optical cavity.[4] While other technqiues have been proposed to selectively form the endo or exo products, this novel pathway opens new directions for organic and inorganic synthesis which may pave the way for chemistry beyond what is currently acessible.

We use the quantum mechanical description of the molecule-cavity hybrid system using the Pauli-Fierz Hamiltonian in the dipole gauge,[5–7] as shown in the following Eq. 1, to investiagte how cavity vacuum fluctuations induce modifications to the

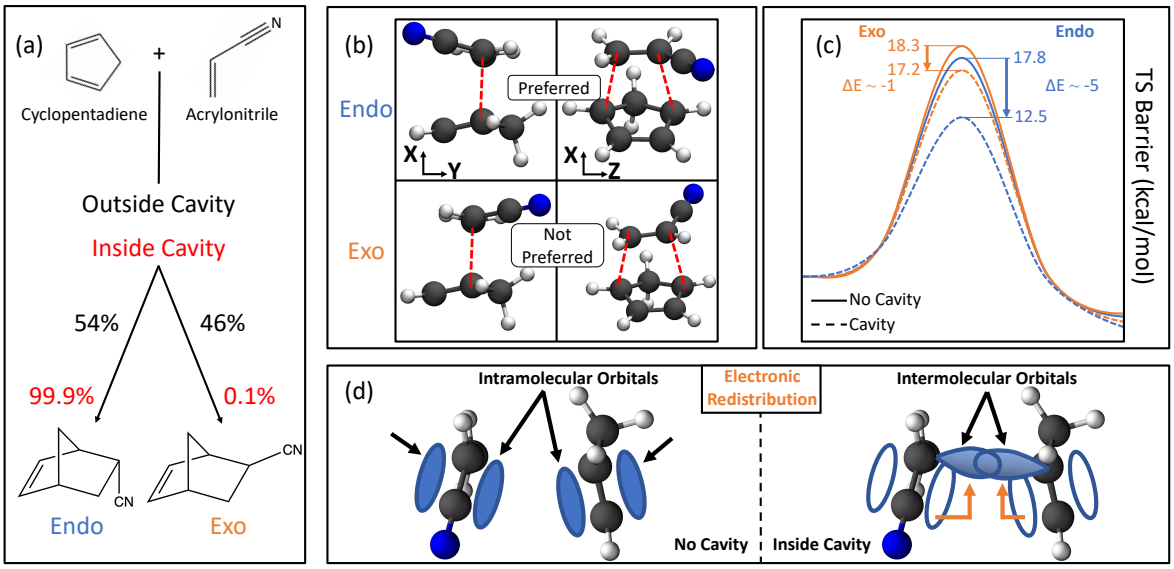

Scheme 1: (a) Schematic representation of the Diels-Alder reaction between cyclopentadiene and acrylonitrile. The percent distribution of products are shown for outside (black) and inside (red) the cavity.[4] (b) Transition state (TS) geometries for both Endo (top) and Exo (bottom) pathways at two different orientations. (c) The TS barrier energy inside (dashed) and outside (solid) for the Endo (orange) and Exo (blue) reaction pathways. The cavity polarization is aligned with the Y-direction with light-matter coupling strength $A_0 = 0.3$ a.u. and $\omega_c = 1.5$ eV. (d) Schematic illustration showing the cavity-induced redistribution of electron density from intramolecular orbitals to intermolecular ones, thus facilitating an intermolecular bond and lowering the TS barrier energy.

ground state.[4,5,7–11,11–21]

$$\hat{H}_{\rm PF} = \hat{H}_{\rm el} + \hat{H}_{\rm ph} + \omega_c A_0 \hat{\boldsymbol{\mu}} \cdot \hat{\mathbf{e}}(\hat{a}^\dagger + \hat{a}) + \omega_c A_0^2 (\hat{\boldsymbol{\mu}} \cdot \hat{\mathbf{e}})^2 \quad (1)$$

$\hat{H}_{\rm el}$ is the electronic Hamiltonian under the Born-Oppenheimer approximation, which is without the nuclear kinetic energy operator, $\hat{H}_{\rm ph} = \omega_c \hat{a}^\dagger \hat{a}$ is the Hamiltonian of the cavity field, $\hat{a}^\dagger$ and $\hat{a}$ are the raising and lowering operators of the cavity field, $\hat{\mathbf{e}}$ is a unit vector indicating the field polarization direction, and $\hat{\boldsymbol{\mu}}$ is the dipole operator of the molecule. The last two terms are the direct light-matter coupling $\hat{H}_{\rm el-ph}$ and the dipole-self energy (DSE) $\hat{H}_{\rm DSE}$, respectively. Moreover, the light-matter coupling strength is expressed as

$$A_0 = \sqrt{\frac{1}{2\omega_c \epsilon \mathcal{V}}}, \quad (2)$$

where ϵ is the permittivity inside the cavity, and $\mathcal{V}$ is the effective mode volume. Alternatively, the electric field strength $\varepsilon = \omega_c A_0$ can be used as a measure of coupling strength, which is common in experiment. In state-of-the-art cavity designs, such as those from gold or silver NPoM cavities, the local electric field can vary from 1 to 10 V/nm,[22] which is well within the cavity parameters used in the present work (to be discussed in more detail later).

In other words, the following two couplings in the Hamiltonian[5–7] shown in Eq. 1 cause the polariton ground states modifications. First, the off-resonance light-matter term ($\hat{H}_{\rm el-ph}$) couples through the ground state permanent dipole and transition dipoles between the ground and excited states. One simple example for the first case is the coupling between $|\psi_g, 0\rangle$ and $|\psi_g, 1\rangle$, which is proportional to $\langle\psi_g, 0|\hat{\mu}(\hat{a}^\dagger + \hat{a})|\psi_g, 1\rangle = \mu_{gg}\langle 0|(\hat{a}^\dagger + \hat{a})|1\rangle = \mu_{gg}$, and $|\psi_g, 1\rangle$ will further couple to $|\psi_e, 0\rangle$ through $\langle\psi_e, 0|\hat{\mu}(\hat{a}^\dagger + \hat{a})|\psi_g, 1\rangle = \mu_{ge}\langle 0|(\hat{a}^\dagger + \hat{a})|1\rangle$, where μ_{gg} and μ_{ge} are the permenant and transition dipoles among the ground and excited states, each projected along the cavity polariation direction $\hat{\mathbf{e}}$. Excited polariton states Φ_e are formed when the $|\psi_g, 1\rangle$ and $|\psi_e, 0\rangle$ states become close in energy and hybridize.[11]

The second contribution is from dipole self-energy ($\hat{H}_{\rm DSE}$), which does not couple states of varying photon number but which does provide non-trivial electronic couplings between ground and excited states. The DSE terms that cou-

ple to the ground state are proportional to $\langle\psi_g|\hat{\mu}^2|\psi_\alpha\rangle = \sum_\gamma \mu_{g\gamma}\mu_{\gamma\alpha}$, where α and γ include the ground and all excited electronic states. Overall, the direct coupling term $\hat{H}_{\mathrm{el-ph}}$ and $\hat{H}_{\mathrm{DSE}}$ both contribute to modifications to the ground state.[10–12,23–26] Through these non-resonant light-matter couplings, the cavity induces modifications to the reactions that are beyond the prediction of the simple Jaynes-Cummings model.[27]

In this work, we demonstrate that the strong coupling between molecule and cavity can fundamentally change a grudn state DA reaction. We apply the recently developed *ab initio* polariton chemistry approach,[11] and theoretically demonstrate that one can fundamentally change the selectivity of this reaction from non-selective endo/exo products to highly selective endo/exo products by coupling this reaction inside an optical cavity. We chose $\omega_{\mathrm{c}} = 1.5$ eV and the coupling strength $A_0 = 0.3$ a.u. that is equivalent to a mode volume $\mathcal{V} \sim 0.19$ nm^3 and field intensity of $\mathcal{E} \sim 8.50$ V/nm, which the cavity frequency and field strength are experimentally achievable for plasmonic nano-cavity parameters.[22] We provide a direct comparison to an alternative formulation of *ab initio* QED[4] for the same reaction. We also provide additional chemical insight, beyond that which was provided in Ref. 4, into the cavity-induced changes to the ground state electron density[13] and relate the changes in density to the interplay between inter- and intra-molecular bonding orbitals (see Fig. 1d), which are commonly used in the description of bond formation.[21] Furthermore, we extend the previous results by computing all possible orientations of the molecule with respect to the cavity field polarization directions and show that the maximum selectivity is not along the previously explored polarization directions. Hence, we show that strong couplings between molecules inside the cavity offer a promising tool[21] that comes with direct chemical intuition via cavity-induced ground state electron density changes to fundamentally modify the outcome of a known chemical reactions, making otherwise non-selective reactions selective.

Theoretical Methods.

We use the *ab initio* polariton approach, called parametrized-QED (pQED)[11] to perform the calculations. The pQED approach uses Pauli-Fierz Hamiltonian in the Born-Oppenheimer approximation (see Eq. 1) to describe light and matter interactions and use adiabatic electronic states as the basis for the electronic degrees of freedom, and Fock states as the basis for the photonic DOF.

The polariton eigenstates and eigenenergies are obtained by solving the following equation

$$\hat{H}_{\mathrm{PF}}|\Phi_j(\mathbf{R})\rangle = E_j(\mathbf{R})|\Phi_j(\mathbf{R})\rangle, \tag{3}$$

where $\hat{H}_{\mathrm{PF}}$ is given in Eq. 1, $E_j(\mathbf{R})$ is the Born-Oppenheimer polaritonic potential energy surfaces (which parametrically depend on the nuclear coordinates $\mathbf{R}$), and $|E_j(\mathbf{R})\rangle$ is the polariton state. We directly diagonalize the polaritonic Hamiltonian $\hat{H}_{\mathrm{PF}}$ matrix and obtain the eigenvalues. The basis is constructed using the tensor product of electronic adiabatic states $|\psi_\alpha(\mathbf{R})\rangle$ (*i.e.*, eigenstates of the electronic Hamiltonian $\hat{H}_{\mathrm{el}}|\psi_\alpha(\mathbf{R})\rangle = \mathcal{E}_\alpha(\mathbf{R})|\psi_\alpha(\mathbf{R})\rangle$) and the Fock states $|n\rangle$ (*i.e.*, eigenstates of the photonic Hamiltonian $\hat{H}_{\mathrm{ph}}|n\rangle = n\omega_{\mathrm{c}}|n\rangle$), expressed as $|\psi_\alpha(\mathbf{R})\rangle \otimes |n\rangle \equiv |\psi_\alpha(\mathbf{R}), n\rangle$. This basis is used to evaluate the matrix elements of $\hat{H}_{\mathrm{PF}}$, and diagonalizing it provides $E_j(\mathbf{R})$ and the corresponding polariton states

$$|\Phi_j(\mathbf{R})\rangle = \sum_{\alpha}^{\mathcal{N}_{\mathrm{el}}} \sum_{n}^{\mathcal{N}_{\mathrm{F}}} C^j_{\alpha n}|\psi_\alpha(\mathbf{R}), n\rangle, \tag{4}$$

where $C^j_{\alpha n} = \langle\psi_\alpha(\mathbf{R}), n|\Phi_j(\mathbf{R})\rangle$. Here, the number of included electronic states, $\mathcal{N}_{\mathrm{el}}$, and photonic Fock/number states, $\mathcal{N}_{\mathrm{F}}$, are treated as convergence parameters.

In this Diels-Alder reaction, the numbers of states we used to solve the Eq. 3 are $\mathcal{N}_{\mathrm{F}} = 10$ and $\mathcal{N}_{\mathrm{el}} = 50$. We use the light-matter coupling strength $A_0 = 0.3$ a.u. and coupling frequency $\omega_{\mathrm{c}} = 1.5$ eV to perform the reaction. Further details regarding the pQED approach and higher coupling frequency results are provided in the **Supporting Information**.

All electronic structure computations were executed using the QCHEM software package.[28] We employed the parametrized quantum electrodynamics time-dependent density functional theory (pQED-TD-DFT) approach with the ωB97XD hybrid exchange-correlation functional and the 6-311+G** basis set. The cavity polarization direction $\hat{\mathbf{e}}$'s alignment with a specific molecular axis, either $\hat{\mathbf{e}} = \mathbf{X}$ or $\hat{\mathbf{e}} = \mathbf{Y}$, or $\hat{\mathbf{e}} = \mathbf{Z}$; the example orientation is illustrated in Fig. 1. Accordingly, the

matrix elements $\langle\psi_\alpha|\hat{\boldsymbol{\mu}}\cdot\mathbf{X}|\psi_\gamma\rangle$ and $\langle\psi_\alpha|\hat{\boldsymbol{\mu}}\cdot\mathbf{Y}|\psi_\gamma\rangle$ are input for the interaction term $\hat{\boldsymbol{\mu}}\cdot\hat{\mathbf{e}}$ and for the DSE term. For the cavity polarization direction $\hat{\mathbf{e}}$ with respect to the $\mathbf{X}$, $\mathbf{Y}$, and $\mathbf{Z}$ directions of the molecule (see Fig. 4), the interaction term follows the relationship $\hat{\mathbf{e}}\cdot\hat{\boldsymbol{\mu}} = \sin\theta\cos\phi\ \mathbf{X}\cdot\hat{\boldsymbol{\mu}} + \sin\theta\sin\phi\ \mathbf{Y}\cdot\ \hat{\boldsymbol{\mu}} + \cos\theta\ \mathbf{Z}\cdot\hat{\boldsymbol{\mu}}$. Both ground state energies and electron density differences were determined using the QCHEM package.[28]

Results and Discussions.

We investigate the DA reaction between cyclopentadiene and acrylonitrile (Scheme 1a). This reaction produces two distinct endo/exo isomers as products. Outside the cavity and under standard reaction conditions, the DA reaction is kinetically controlled and shows a non-selective result with 54% endo to 46% exo products. It has been recently proposed[4] that this intrisically non-selective reaction can be made selective by coupling the ground state of the reacting molecules to an optical cavity with frequency in the range of electronic excitations (*i.e.*, ω_c ∼1-3 eV) in contrast to the recently explored vibrational polaritons (*i.e.*, $\omega_c \sim 0.1$ eV) To explore this effect, we apply the recently developed[11,19] *ab initio* cavity quantum electrodynamics to further investigate this reaction and its properties under strong coupling.

Scheme 1b shows the transition states (TS) of this reaction that lead to the endo (top) and exo (bottom) products. The red dashed lines between the molecules show the bonds that will form upon the creation of the product for clarity. Furthermore, we indicate that the endo pathway becomes preferred inside the cavity under experimentally feasible cavity conditions and under and orientational average of electric field polarization directions. As suggested in Ref. 4 (and reproduced in the current work), the selectivity shifts to 99.9% for the endo product and only 0.1% for the exo. As an example of the modifications to the potential energy surface, we show the ground state potential energy surface in Scheme 1c, where the reactant (R) and TS geometries of the endo (blue) and exo (orange) isomers are placed inside the cavity with the cavity polarization along the Y-direction of the molecule. In tihs case, there is a significant shift in selectivity toward the endo species through a reduction of the TS barrier height by ∼5 kcal/mol for the endo and ∼1 kcal/mol for the exo compared to outside the cavity. This shifts the expected yields of the reaction to 99.9% and 0.1% for the endo and exo isomers, respectively, consistent with those data reported in Ref. 4. In this case, our QED-time-dependent density functional theory (QED-TD-DFT) calculations for the align closely with the QED-coupled cluster singles and doubles (QED-CCSD) approach,[4] with more details and comparisons to be discussed in Fig. 2. This shift in selectivity can be understood as cavity-induced electronic redistribution under the influence of the cavity (Scheme 1d). More specificallty, coupling to the cavity induces electron density to be taken from populated/occupied intramolecular π-bonding orbitals (*i.e.*, single-particle orbitals) to virtual/unoccupied intermolecular orbitals, thus facilitating a reduction in energy of the TS barrier height.

To further provide a benchmark of our QED-TDDFT approach against that of the high-level QED-CCSD provided in Ref. 4, Fig. 1 and Fig. 2 explore the X-, Y-, and Z-directions of cavity field polarization using the TS geometries provided in Ref. 4. Fig. 1 shows the TS barrier height $E^{\ddagger} = E_0(\mathbf{R}_{\mathrm{TS}}) - E_0(\mathbf{R}_{\mathrm{reac}})$ in the ground polaritonic state $|\Phi_0(\mathbf{R})\rangle$ as a function of the light-matter coupling strength A_0 for the three primary cavity field polarization directions, (blue) X, (orange) Y, and (green) Z, for the (a) endo and (b) exo isomers. In both the endo and exo pathways (Fig. 1), the TS barrier increases for the X-polarized cavity (blue curve) by 7.2 kcal/mol and 6.7 kcal/mol at $A_0 = 0.3$ a.u., respectively, compared to outside the cavity ($A_0 = 0.0$ a.u.). The X-polarized cavity is not expected to offer selectivity for this reaction due to the simultaneous and unfavorable increase in TS barrier energy for the two isomers. In contrast, the Y-direction shows a decreases in both the endo (5.3 kcal/mol) and exo (1.3 kcal/mol) pathways. The endo isomer exhibits an additional 3.0 kcal/mol reduction in the TS barrier compared to the exo isomer, thus offering a significant selectivity toward the endo

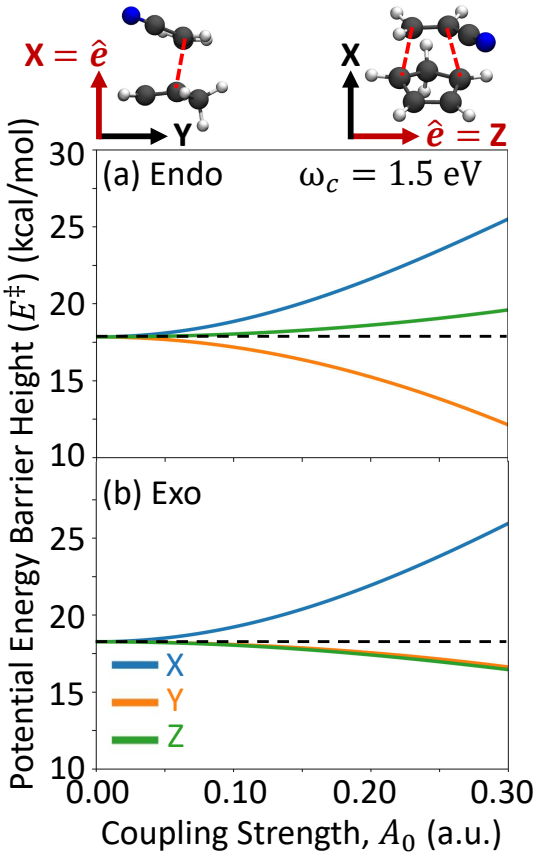

Figure 1: The polaritonic ground state activation energy, defined as the energy difference between the transition state and the reactant geometries, $E^{\ddagger} = E_0(\mathbf{R}_{\rm TS}) - E_0(\mathbf{R}_{\rm reac})$, for the two reaction pathways, (a) Endo and (b) Exo. Here, $E_0(\mathbf{R})$ is the polaritonic ground state energy defined in Eq. 3 at nuclear geometry $\mathbf{R}$. The colors correspond to cavity polarizations along the X- (blue), Y- (orange) and Z-directions (green). The cavity frequency is $\omega_{\rm c} = 1.5$ eV. The horizontal dashed line indicates the uncoupled barrier height (*i.e.*, $A_0 = 0.0$ a.u.).

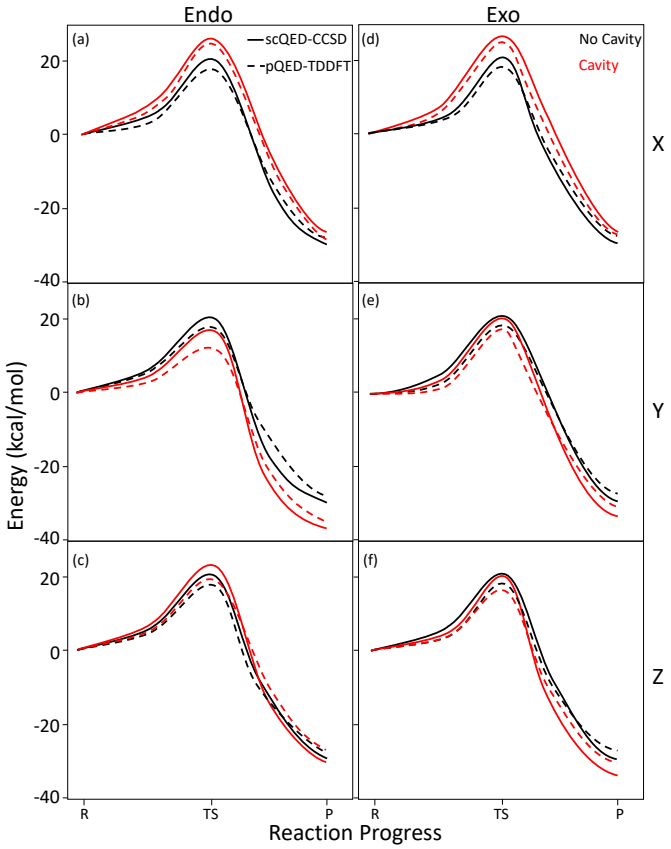

Figure 2: Potential energy surfaces, $E_0(\mathbf{R})$, as functions of the reaction progress from the reactant (R) to the transition state (TS) and to the product (P), inside (red) and outside (black) the cavity for both reaction pathways (a-c) Endo and (d-f) Exo. The (a,d) X-, (b,e) Y-, and (c,f) Z-polarizations of the cavity are shown. The (dashed) pQED-TDDFT approach of the current work is directly compared to the (solid) scQED-CCSD method of Ref. 4. The curves were interpolated between the R, TS, and P data points using a spline approach to improve the visual clarity. The light-matter coupling strength is $A_0 = 0.3$ a.u. with cavity frequency $\omega_{\rm c} = 1.5$ eV.

isomer. The Z-direction also offers a cavity-mediated selectivity, now favoring the exo isomer. In this case, the endo isomer's TS barrier is increased by 1.5 kcal/mol while the exo barrier height is decreased by 1.8 kcal/mol, generating a 3.3 kcal/mol difference in TS barrier height between isomers. In the Y- and Z-polarization cases, we expect the endo product yields to be $\mathcal{P}_{\rm endo} = \exp[-E^{\ddagger}_{\rm endo}/k_{\rm B}T]/\mathcal{Z}$ = 99.9% and 0.4%, respectively, where $\mathcal{Z} = \exp[-E^{\ddagger}_{\rm endo}/k_{\rm B}T] + \exp[-E^{\ddagger}_{\rm exo}/k_{\rm B}T]$. Thus, we have demonstrated that the cavity can offer a novel approach toward the selective isomerization of this DA reaction and that our pQED-TDDFT approach is in agreement with Ref. 4 at the QED-CCSD level.

Fig. 2 presents a more direct comparison between the pQED-TDDFT of the current work using pQED-TDDFT and that of the high-level scQED-CCSD of Ref. 4 by showing the exact QED-TDDFT and QED-CCSD TS barrier energies as well as the product energies with an interpolated spline grid portraying the rest of the potential energy surface as a schematic. In gen-

eral, we find only minor quantitative differences between the two approaches that can be rationalized by the known deviations between standard CCSD and DFT methodologies, which are expected to reach 1-5 kcal/mol. Here, such deviations reach up to 3.0 kcal/mol for the Endo pathway and 2.6 kcal/mol for the Exo pathway, signifying that our pQED-TDDFT is well within the expected error of the bare many-body approach itself.[11] More importantly, our pQED-TDDFT results portray the same qualitative behavior of the endo and exo potential energy surfaces as the scQED-CCSD for all data points except two: the X- and Z-polarization directions for the endo product energies. In the X-polarization direction, the scQED-CCSD approach predicts an increase in energy for the endo product, while our pQED-TDDFT method indicates a slight decrease. In the Z-polarization direction, the scQED-CCSD results show a minor decrease in product energy, whereas the pQED-TDDFT approach shows an increase. A more detailed analysis of these subtle differences is available in the **Supporting Information**. Furthermore, the differences in the QED-CCSD and pQED-TDDFT energies are less than 2 kcal/mol and well within the error expected between the standard TDDFT and CCSD methodologies and thus acceptable for our qualitative exploration of this DA reaction which, for the rest of the work, only focuses on the correctly reproduced TS barrier geometries/energies.

In order to rationalize the observations seen in Fig. 1 and Fig. 2, we extend the work of Ref. 4 to include a chemical rationale for the cavity-induced changes to the ground state reaction barrier. Fig. 3 shows the density difference isosurfaces for the TS geometries for the endo (top) and exo (bottom) isomers for all three principle cavity polariation directions: x (left), Y (middle), and Z (right). The difference density function is defined as $\Delta\rho_{00}(\mathbf{r}) = \rho^{\mathrm{M}}_{00}(\mathbf{r}) - \xi_{00}(\mathbf{r})$, where $\rho^{\mathrm{M}}_{00} = \mathrm{Tr}_{\mathrm{ph}}[\hat{\rho}_{00}] = \mathrm{Tr}_{\mathrm{ph}}[|\Phi_0\rangle\langle\Phi_0|]$ is the total ground state polaritonic density with the photon DOFs traced out. $\xi_{00}(\mathbf{r}) = \psi^*_0(\mathbf{r})\psi_0(\mathbf{r})$ is the bare electronic ground state density. The difference of these two densities portrays the effects of cavity-induced electronic redistribution around the molecule. The regions in which $\Delta\rho_{00}(\mathbf{r}) > 0$ (red colored) indicates that a gain of electron density has occured, and depletion when $\Delta\rho_{00}(\mathbf{r}) < 0$ (blue colored). Additional visualization angles are shown in Fig. S4 in the **Supporting Information**. This effect can be rationalized chemically by considering that the cavity can induce redistribution (exchange of character) between bare occupied and unoccupied single-particle orbitals (*e.g.*, HOMO $\leftrightarrow$ LUMO), which allows for changes to the standard molecular orbital theory inside the cavity.[21]

The X-polarization direction showcased a simultaneous increase in TS barrier energy for the endo and exo isomers (see Fig. 1), thus we expect that the potential chemical bond between the two reactant molecules is weakened by the presence of the cavity for both isomer configurations. Fig. 3a,d show the ground state difference density isosurface for the (Fig. 3a) endo and (Fig. 3d) exo isomers with the cavity polarized along the X-direction of the molecule (see cartesian axes above Fig. 3a). The region between the reactant molecules is blue, which indicates that this region has been depleted of electron density. This region is also responsible for the formation of the intermolecular bond during the reaction. Since this region has lost these intermolecular bonding electrons, the TS geometry has been destabilized compared to outside the cavity. Contrary to this result, the Y-polarization of the cavity induced a stabilization of the TS barrier energy (Fig. 1). Fig. 3b,e show the difference density in this case, and, opposite to Fig. 3a,d, we find an increase in electron density in the region between the reactant species, this strengthening the intermolecular bond at the TS geometry and reducing the TS barrier energy.

The regions of not localized between the reactant species in Fig. 3 are considered as intramolecular density redistributions and are mostly shaped as intramolecular π-bonding orbitals. This is especially evident on the lower molecule (cyclopentadiene). For the X-polarization, these orbitals exhibit electron density accumulation from the intermolecular bonding orbitals. However, for the Y-

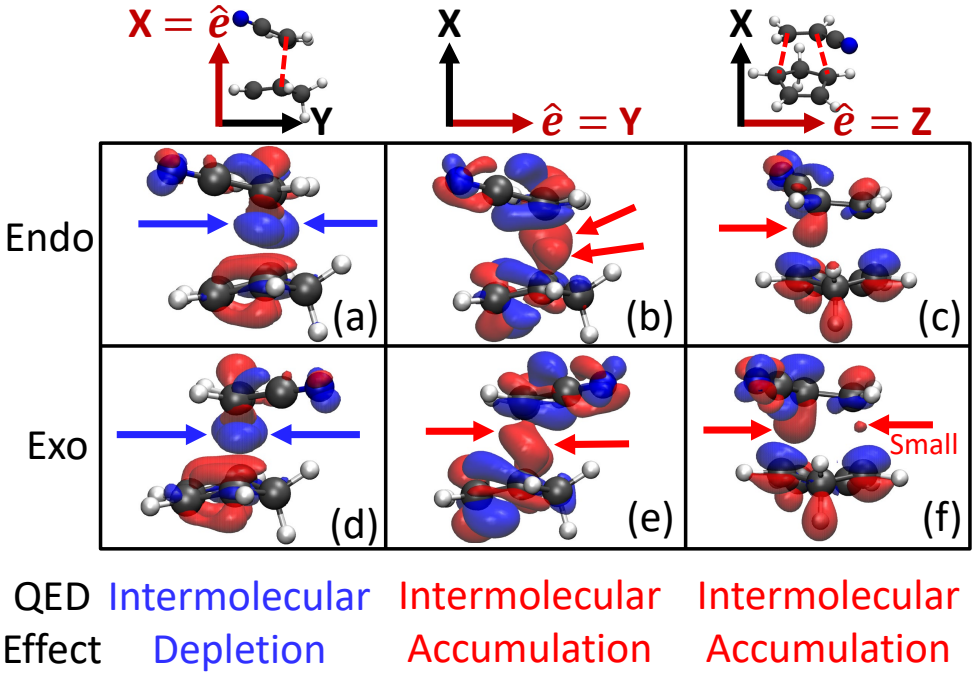

Figure 3: Difference density isosurfaces at the transition state geometries for the (a-c) Endo and (d-f) Exo pathways for cavity polarizations along the (a, d) X-, (b, e) Y-, and (c, f) Z-directions. The isosurfaces in each panel correspond to the difference density, $\Delta\rho_{00}(x,y,z) = \rho^{\mathrm{M}}_{00}(x,y,z) - \xi_{00}(x,y,z)$, at the transition state geometry using the pQED-TDDFT approach of the current work. Each panel corresponds to potential energy surface diagrams in Fig. 2 (pQED-TDDFT method part). The color indicates the accumulation (red) or depletion (blue) of electron density upon insertion into the cavity. The arrows indicate the intermolecular bonding orbitals. In all cases, the light-matter coupling strength $A_0 = 0.2$ a.u. with cavity frequency $\omega_c = 1.5$ eV. The isovalue chosen for the X-direction is 1.0 m|e|/Å^2 and 0.2 m|e|/Å^2 for the Y- and Z-polariations, where m|e| = |e|×1000 and |e| is the charge of an electron.

polarization, these intramolecular π-bonding orbitals donate their electrons to the intermolecular bond. Thus, the effects of the cavity are to induce changes to the bonding structure of the reactant species, thus either facilitating or disallowing the bond formation depending on the cavity polarization direction.

The Z-polarization direction is weakly changing the TS barrier energy (Fig. 1) and oppositely between the endo and exo isomers. Notably, the difference density in this case (Fig. 3c,f) exhibits weaker and asymetric changes to the intermolecular region. Note that the molecule is rotated by 90 degrees about the X-axis in Fig. 3c,f compared to Fig. 3a,b,d,e for visual clarity. Additionally, the intramolecular density, especially on the bottom molecule (cyclopentadiene) shows a different symmetry compared to those shown in Fig. 3a,b,d,e where the under side of the intramolecular π-bonds are accumulating electron density while the top side are being depleted. Overall, the redistribution of electron density does not facilitate the formation of the two covalent bonds and thus showcases a weaker change to the TS barrier height compared to the X- and Y-polarization directions.

Overall, we have used the differnece density function to develop a chemically appealing interpretation of the DA reaction between cyclopentadiene and acrylonitrile. While this reaction was previously explored with the high-level scQED-CCSD approach, we have extended this work to incorporate a relavent chemical explanation in terms of the cavity-mediated redistribution of inter- and intramolecular bonding orbitals by examing the polaritonic ground state density. These orbitals are explicitly modified by the cavity to facilitate the formation (or destruction) of

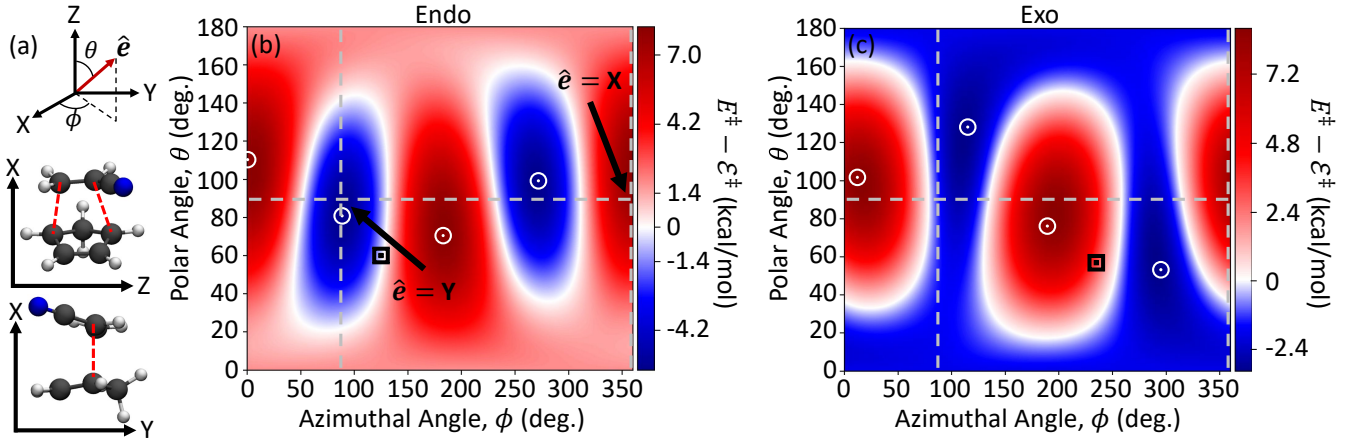

Figure 4: (a) A schematic of the spherical coordinate system with an arbitrary cavity polarization vector $\hat{e}(\phi,\theta)$ and two orientations of the molecule with respect to the primary cartesian axes. (b,c) The difference between the polaritonic transition state barrier, $E^{\ddagger} = E_0(\mathbf{R}_{\mathrm{TS}}) - E_0(\mathbf{R}_{\mathrm{reac}})$, and the barrier of the bare molecular system, $\mathcal{E}^{\ddagger} = \mathcal{E}_0(\mathbf{R}_{\mathrm{TS}}) - \mathcal{E}_0(\mathbf{R}_{\mathrm{reac}})$, for the (b) Endo and (c) Exo reaction pathways as functions of the azimuthal ϕ and polar θ angles. The colorbar indicates the sign and magnitude of the difference of the energy barrier height, $E^{\ddagger} - \mathcal{E}^{\ddagger}$. The blue regions indicate where the transition state barrier is lowered compared to outside the cavity. The white symbols indicate the maxima and minima values, with only two non-degenerate points on each pathway and are related to the other set by symmetry. We found the maximum and minimum critical points for the Endo pathway to be $(\phi_1,\theta_1) = (\phi_{\mathrm{MAX}}^{\mathrm{ENDO}},\theta_{\mathrm{MAX}}^{\mathrm{ENDO}}) = (3.3^{\circ},111.2^{\circ})$ and $(\phi_2,\theta_2) = (\phi_{\mathrm{MIN}}^{\mathrm{ENDO}},\theta_{\mathrm{MIN}}^{\mathrm{ENDO}}) = (91.7^{\circ},80.2^{\circ})$; for Exo pathway, the points are $(\phi_3,\theta_3) = (\phi_{\mathrm{MAX}}^{\mathrm{EXO}},\theta_{\mathrm{MAX}}^{\mathrm{EXO}}) = (11.5^{\circ},103.1^{\circ})$ and $(\phi_4,\theta_4) = (\phi_{\mathrm{MIN}}^{\mathrm{EXO}},\theta_{\mathrm{MIN}}^{\mathrm{EXO}}) = (114.6^{\circ},126.1^{\circ})$, respectively. The black square symbols indicate the ground state dipole moment unit vectors, $\vec{\mu}_{00}$, for the endo and exo pathways, which are (b) $(125.6^{\circ},60.8^{\circ})$ and (c) $(235.7^{\circ},56.9^{\circ})$, respectively. For both panels, the light-matter coupling strength $A_0 = 0.3$ a.u. and cavity frequency $\omega_{\mathrm{c}} = 1.5$ eV.

the intermolecular bond by donating electron density from intramolecular π-orbitals (largely localized on the cyclopentadiene species) to the forming intermolecular bond.

The cavity polarization directions along the principle cartesian axes (X, Y, and Z) were taken as a benchmark from the previous work of Ref. 4; however, we point out that the use of these cartesian directions as "important" field polarization directions is a choice. In reality, choosing a useful, chemically relavent coordinate system is very difficult in general, and the effects of the cavity may not straightforwardly connect to our understanding of the chemistry of a certain molecule or reaction between molecules. With this in mind, we extend our exploration to an arbitrary cavity field polarization vector $\hat{e} = \hat{e}(\phi,\theta)$, where ϕ and θ are the azimuthal and polar angles, respectively, defined schematically in Fig. 4a. Fig. 4b and Fig. 4c show the change in TS barrier energy $\Delta E^{\ddagger}(\phi,\theta) = E^{\ddagger}(\phi,\theta) - \mathcal{E}^{\ddagger}$ for the endo and exo isomer, respectively, with light-matter coupling strength $A_0 = 0.3$ a.u. and cavity frequency $\omega_{\mathrm{c}} = 1.5$ eV. Here, $E^{\ddagger}(\phi,\theta)$ is the polaritonic ground state TS barrier energy and $\mathcal{E}_0$ is the bare electronic ground state TS barrier energy (equivalent to $E^{\ddagger}$ with $A_0 = 0.0$ a.u. and $\omega_{\mathrm{c}} = 0.0$ eV). The negative regions indicate a reduction in the TS barrier height inside the cavity, while the red regions show an increase to the TS barrier height.

The endo isomer (Fig. 4b) exhibits clear points at which the TS barrier energy is maximized (white circle in the red region) and minimized (white circle in the blue region) for this choice of cavity parmeters. We define these critical points as $(\phi_1,\theta_1) = (3.3^{\circ},111.2^{\circ})$ and $(\phi_2,\theta_2) = (91.7^{\circ},80.2^{\circ})$, respectively. Connecting to the previous figures, the X- and Y-directions are equivalent to $(\phi,\theta) = (0^{\circ},90^{\circ}) = (360^{\circ},90^{\circ})$ and $(\phi,\theta) = (90^{\circ},90^{\circ}) = (270^{\circ},90^{\circ})$, respectively. In the endo case (Fig. 4b), the X- and Y-polarization directions are near to

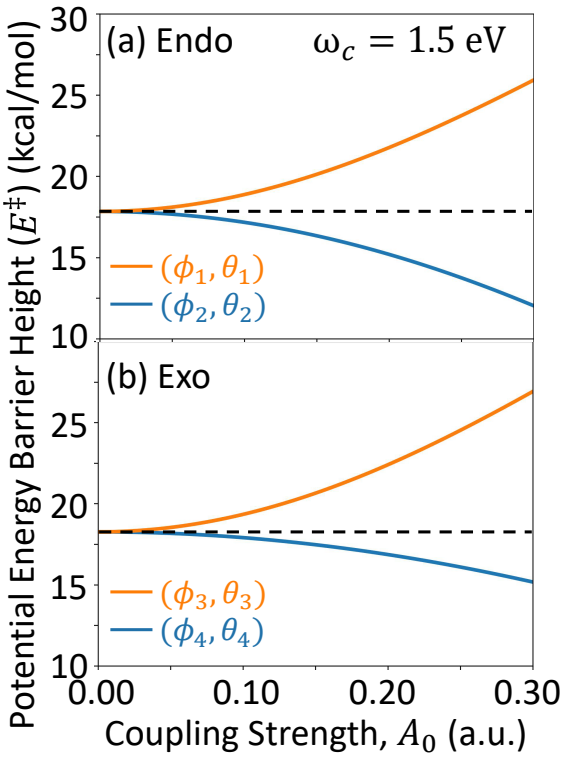

Figure 5: The polaritonic ground state activation energy, defined as the energy difference between the transition state and the reactant geometries, $E^\ddagger = E_0(\mathbf{R}_{\mathrm{TS}}) - E_0(\mathbf{R}_{\mathrm{reac}})$, for the two reaction pathways, (a) Endo and (b) Exo. The cavity polarizations are shown at the critical points for each pathway: (ϕ_1, θ_1) and (ϕ_3, θ_3) (MAX in orange); (ϕ_2, θ_2) and (ϕ_4, θ_4) (MIN in blue). The cavity frequency is $\omega_c = 1.5$ eV. The horizontal dashed line indicates the uncoupled barrier height (*i.e.*, $A_0 = 0.0$ a.u.).

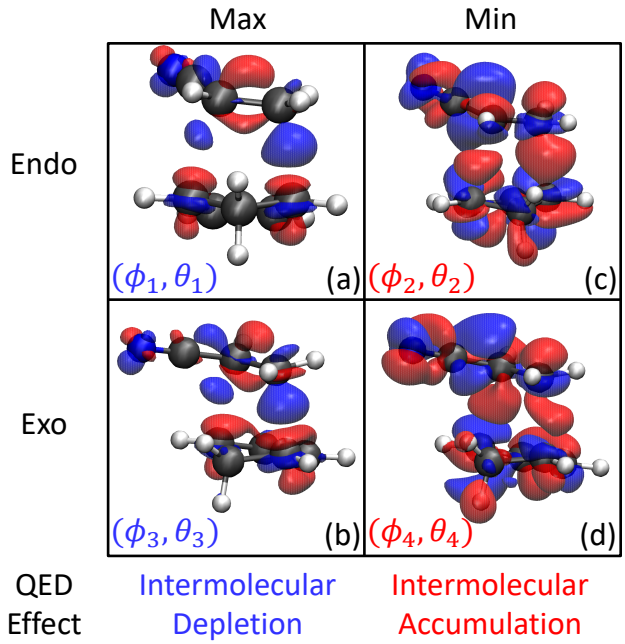

Figure 6: Difference density isosurfaces at the transition state geometries for the (top) Endo and (bottom) Exo pathways. The cavity polarizations are shown at the critical points for each pathway: (a) MAX, Endo pathway (ϕ_1, θ_1); (b) MAX, Exo pathway (ϕ_3, θ_3); (c) MIN, Endo pathway (ϕ_2, θ_2); (d) MIN, Exo pathway (ϕ_4, θ_4). The color indicates the accumulation (red) or depletion (blue) of electron density upon insertion into the cavity. The arrows indicate the intermolecular bonding orbitals. In all cases, the light-matter coupling strength $A_0 = 0.2$ a.u. with cavity frequency $\omega_c = 1.5$ eV. The isovalue chosen for both maxima is 1.0 m|e|/Å^2 and 0.2 m|e|/Å^2 for the minima, where m|e| = |e|×1000 and |e| is the charge of an electron.

the critical points (ϕ_1, θ_1) and (ϕ_2, θ_2). However, for the exo isomer (Fig. 4c), the critical points are located at $(\phi_3, \theta_3) = (11.5°, 103.1°)$ and $(\phi_4, \theta_4) = (114.6°, 126.1°)$. Hence, the Y-axis direction is far from either of the extrema for the exo case. In fact, the Y-direction lies on the border between the stabilizing region (blue) and the destabilizing region (red). In both cases, the Z-direction is far from any critical point, implying that this direction of cavity polarization is not optimal in either isomer. Later, in Fig. 7 that the Z-polarization can still be valuable in cavity-induced selectivity even though both isomers experience a mediocre cavity effect individualy.

Similarly to Fig. 1, Fig. 5 shows the TS barrier energy $E^\ddagger$ as a function of the light-matter coupling strength A_0 for the above-mentioned critical angles for the cavity polarization vector (ϕ_i, θ_i) for both isomers. The cavity frequency is $\omega_c = 1.5$ eV. It is evident that the (ϕ_1, θ_1) and (ϕ_3, θ_3) maximize the individual isomer TS barrier energies while the (ϕ_2, θ_2) and (ϕ_4, θ_4) minimize this energy for all values of coupling strength A_0. In turn, we can inspect the ground state difference density isosurfaces for these critical points, as shown in Fig. 6. As expected, the polarization angles that maxi-

mize the TS barrier energy contain intermolecular electron density depletion, destabilizing the forming bond, as well as electron accumulation in the intramolecular bonding π-orbitals of each reactant molecule. The opposite is again true for the angles that minimize the TS barrier energy, showing electron density accumulation in the intermolecular bonding region. Notably, the intramolecular π-bonding orbitals showcase asymetric accumulation/depletion, similar to the Z-polarization in Fig. 3c,f. We hypothesize that these critical angles of the field induce a complicated redistribution of electron density, not only from the reactant species to the forming intermolecular bond, but also among themselves in a way that further decreases the energy of the TS geometry. Hence, examining only the principle directions X, Y, and Z as defined by chemical intuition will mostly likely not showcase the maximal effects of the complicated electron-photon correlation (as the black square symbols shown in Fig. 4) since the direction of the many coupled permenant and transition dipole matrix elements in the adiabatic electronic basis is not straightforward and likely does not relate to a simple and meaningful chemical property.

To fully control the chemical reaction, the relative TS barrier energies between the endo and exo isomers must be controlled. Fig. 7a presents the TS barrier energy difference, $E^{\ddagger}_{\mathrm{Endo}} - E^{\ddagger}_{\mathrm{Exo}}$, as a function of the cavity polarization direction (ϕ, θ) for a fixed cavity frequency $\omega_{\mathrm{c}} = 1.5$ eV and light-matter coupling strength $A_0 = 0.3$ a.u. This presentation of the data is different than that of Fig. 4, which depicted only the Endo or Exo barrier height change with respect to outside the cavity, *e.g.*, $E^{\ddagger}_{\mathrm{Endo}} - \mathcal{E}^{\ddagger}_{\mathrm{Endo}}$, but not the energy difference between the barrier heights of the two isomers, $E^{\ddagger}_{\mathrm{Endo}} - E^{\ddagger}_{\mathrm{Exo}}$. Thus, Fig. 7 is related to the probability of forming either Endo or Exo species at a given orientation with respect to the cavity field direction. Negative values of this quantity (blue regions) indicate parameter regimes where the endo pathway is lower in energy compared to the exo pathway. Contrary to this, positive values indicate regions where the exo pathway is lower in energy. The cavity polarization angles at which the highest amount of selectivity toward the endo, $(\phi_{\mathrm{Endo}}, \theta_{\mathrm{Endo}}) = (68.8°, 80.2°)$ at 5.88 $\mathrm{k_B T}$, and exo, $(\phi_{\mathrm{Exo}}, \theta_{\mathrm{Exo}}) = (137.5°, 160.4°)$ at -10.73 $\mathrm{k_B T}$, pathways are the critical points of the function $E^{\ddagger}_{\mathrm{Endo}} - E^{\ddagger}_{\mathrm{Exo}}$. These angles are shown as white circle-dots in Fig. 7a.

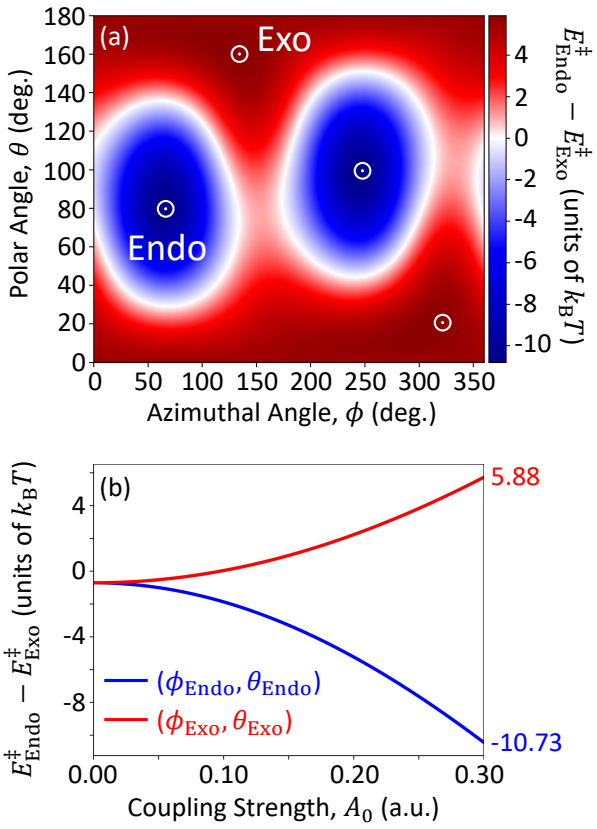

Figure 7: (a) TS barrier energy difference between the Endo and Exo isomers, $E^{\ddagger}_{\mathrm{Endo}} - E^{\ddagger}_{\mathrm{Exo}}$, as a function of the cavity polarization direction, (ϕ, θ). The blue region ($E^{\ddagger}_{\mathrm{Endo}} < E^{\ddagger}_{\mathrm{Exo}}$) indicates that the Endo pathway has a lower TS barrier energy and is preferable compared to the Exo pathway; the red region, in contrast, indicates that the Exo pathway is preferable. The light-matter coupling strength $A_0 = 0.3$ a.u. and the cavity frequency $\omega_{\mathrm{c}} = 1.5$ eV. The white circle-dot symbols indicate the critical points at which $E^{\ddagger}_{\mathrm{Endo}} - E^{\ddagger}_{\mathrm{Exo}}$ is maximized, $(\phi_{\mathrm{Exo}}, \theta_{\mathrm{Exo}}) = (137.5°, 160.4°)$, or minimized, $(\phi_{\mathrm{Endo}}, \theta_{\mathrm{Endo}}) = (68.8°, 80.2°)$, offering the maximum amount of selectiveity for the Exo and Endo isomers, respectively. (b) TS barrier energy difference between the Endo and Exo isomers, $E^{\ddagger}_{\mathrm{Endo}} - E^{\ddagger}_{\mathrm{Exo}}$ as a function of the light-matter coupling strength at the critical angles which produce the maximal selectivity of endo (blue) and exo (red) isomers.

In experiment, control over the light-matter coupling strength A_0 is difficult and is often susceptible to many environmental factors. While our calculations predict strong selectivity at these critical angles of cavity polarization direction, the selectivity at weaker light-matter coupling strengths A_0 may provide a deeper insight into experimental observations. Fig. 7b presents the TS barrier energy difference, $E^{\ddagger}_{\mathrm{Endo}} - E^{\ddagger}_{\mathrm{Exo}}$, as a function of the light-matter coupling strength A_0 for both of the critical angles shown in Fig. 7a. At small values of light-matter coupling ($A_0 < 0.05$ a.u.), negligible selectivity is predicted. Our calculations predict that, at these critical angles, prominent endo selectivity can be achieved at or above $A_0 = 0.10$ a.u. at which the TS barrier energy difference is greater than 2 k_BT at room temperature. For the exo isomer, the selectivity is weaker and requires at least $A_0 = 0.20$ a.u. for the same degree of selectivity induced by the TS barrier energy difference. Hence, in the experiment, strong selectivity in thie reaction is already achievable with current plasmonic cavity designs.[22]

Furthermore, while possible,[29] it is often difficult to control the orientation of the molecules with respect to the cavity's electric field polarization (ϕ, θ). In experiment, we expect random orientation of the molecules during the reaction, so we calculate the angular average of the energy differences shown in Fig. 7a,

$$\langle E^{\ddagger}_{\mathrm{Endo}} - E^{\ddagger}_{\mathrm{Exo}} \rangle = \frac{\iint d\phi\, d\theta\, (E^{\ddagger}_{\mathrm{Endo}} - E^{\ddagger}_{\mathrm{Exo}}) \sin(\theta)}{\iint d\phi\, d\theta\, \sin(\theta)} \tag{5}$$

Here, $\langle E^{\ddagger}_{\mathrm{Endo}} - E^{\ddagger}_{\mathrm{Exo}} \rangle$ = -0.9212 k_BT, which implies that, on average, the Endo pathway is preferred by nearly k_BT at room temperature. Hence, we have theoretically shown that this DA reaction will provide appreciable selectivity inside the cavity, even if the orientation of the molecules cannot be controlled.

In our final discussion, we seek to further understand the fundamental contributions to the cavity-induced selectivity of this DA reaction. Fig. 8 presents the contributions of each Hamiltonian component to the TS barrier energies at the critical cavity polarization angles for the endo (Fig. 8a,c) and exo (Fig. 8b,d) isomers. The energy contributions are calculated as $E^{\ddagger}_a = \langle \Phi_0(\mathbf{R}_{\mathrm{TS}}) | \hat{H}_a | \Phi_0(\mathbf{R}_{\mathrm{TS}}) \rangle - \langle \Phi_0(\mathbf{R}_{\mathrm{reac}}) | \hat{H}_a | \Phi_0(\mathbf{R}_{\mathrm{reac}}) \rangle$, where $\hat{H}_a \in \{\hat{H}_{\mathrm{PF}}, \hat{H}_{\mathrm{el}}, \hat{H}_{\mathrm{ph}}, \hat{H}_{\mathrm{el-ph}}, \hat{H}_{\mathrm{DSE}}\}$. $|\Phi_0(\mathbf{R})\rangle$ is the ground state polaritonic wavefunction, always defined by the total PF Hamiltonian $\hat{H}_{\mathrm{PF}} |\Phi_0(\mathbf{R})\rangle = E_0(\mathbf{R}) |\Phi_0(\mathbf{R})\rangle$ (Eq. 3). These contributions are shown for each of the four cavity polarization directions defined in Fig. 4: (Fig. 8a) (ϕ_1, θ_1), (Fig. 8b) (ϕ_3, θ_3), (Fig. 8c) (ϕ_2, θ_2), and (Fig. 8d) (ϕ_4, θ_4). These angles represent the largest (Fig. 8a,b) increase and (Fig. 8c,d) decrease in the transition state barrier height for the (Fig. 8a,c) endo and (Fig. 8b,d) exo isomers. The cavity frequency $\omega_c = 1.5$ eV. In the **Supporting Information**, Fig. S5 and Fig. S6 present the same data but for the reactant and TS geometries individually.

By construction, the total energy $\hat{H}_{\mathrm{PF}}$ (solid black) for (ϕ_1, θ_1) and (ϕ_3, θ_3) increases as a function of the light-matter coupling strength and decreases for (ϕ_2, θ_2) and (ϕ_4, θ_4). Of most importance and interest are the two interaction terms $\hat{H}_{\mathrm{el-ph}}$ (solid red) and $\hat{H}_{\mathrm{DSE}}$ (solid gold), which are responsible for the modifications to the TS barrier energy $E^{\ddagger}$ inside the cavity. For both critical angles at which the TS barrier energy is maximized (Fig. 8a,b), the DSE contributes positively to the energy while the direct electron-photon interaction provides a negative contribution. Note that the energy of the DSE for a single-molecule coupled to a cavity is a positive contribution while the direct interaction term is negative. Here we are showing the energy difference between two nuclear geometries, $E^{\ddagger} = E_{\mathrm{TS}} - E_{\mathrm{reac}}$, for which the contribution of either term can be positive or negative (see Fig. S5 and Fig. S6 in the **Supporting Information** for the absolute energies of each term). For the critical angles which the TS barrier energy is minimized (Fig. 8c,d), the opposite trends are observed, where the DSE contributes negatively while the direct interaction term is positive. Additionally, the magnitudes of all terms are reduced since the cavity-induces TS barrier decreases (negative values/blue in Fig. 4) are less in mag-

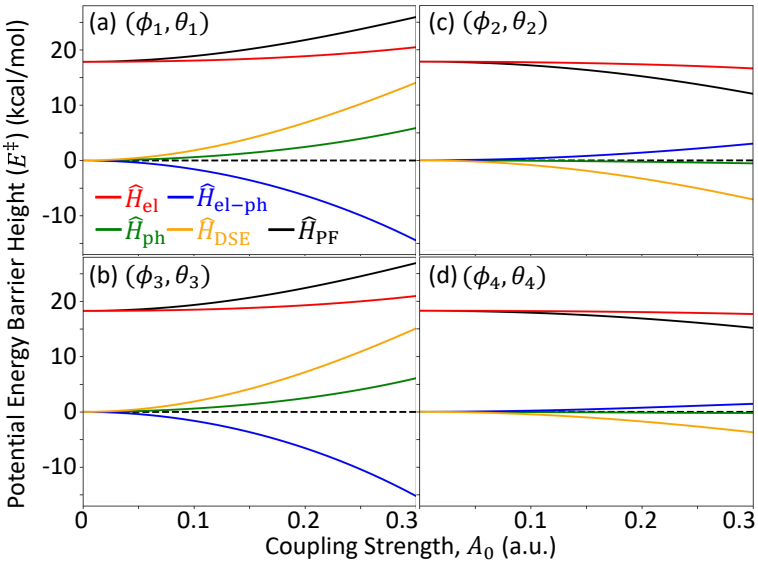

Figure 8: Energy Contributions to the ground state energy barrier height. It shows different energy contributions towards the total Hamiltonian $\hat{H}_{\rm PF}$, which is in black solid curved line. Components are $\hat{H}_{\rm el}$ in red, $\hat{H}_{\rm el-ph}$ in blue, $\hat{H}_{\rm ph}$ in green and $\hat{H}_{\rm DSE}$ in yellow. The horizontal dashed line indicates the uncoupled barrier height (*i.e.*, $A_0 = 0.0$ a.u.). Note that $\hat{H}_{\rm el}$ starts at the same barrier height as $\hat{H}_{\rm PF}$ since we treated the molecular Hamitonian at that zero-point level. Overall, $\hat{H}_{\rm DSE}$ contributes the most to the total energy. The cavity frequency is $\omega_{\rm c} = 1.5$ eV. Absolute barrier energies for reactant and transition state are provided in the **Supporting Information**.

nitude than the cavity-induced increases (positive values/red in Fig. 4).

The energy contributions from $\hat{H}_{\rm el}$ (solid red curve) and $\hat{H}_{\rm ph}$ (solid green curve) terms are activated indirectly by the coupling terms and are more difficult to attribute to simple physics, except that as the absolute energy of $\hat{H}_{\rm el}$ and $\hat{H}_{\rm ph}$ increases in a given nuclear configuration (see Fig. S5 and Fig. S6 in the **Supporting Information** for the absolute energies of the reactant and TS geometries), increasing the contribution from higher-lying electronic excited states and higher photon number states to the polaritonic ground state. In all four cases of critical angles (in Fig. S5 and Fig. S6 as well as their differences shown in Fig. 8), the cavity-induced changes to these terms is smaller than the ther direct electron-photon interaction and DSE terms (see Fig. 4).

At the mean-field level, and in the coherent state representation,[30] it is commonly understood that the DSE is the leading contribution to the cavity-induced changes to the ground state.[5,13,15,16,24] In this representation, the direct electron-photon term is shifted away, leaving only a modified DSE term proportional to the dipole fluctuations $\langle(\Delta\hat{\mu})^2\rangle_{\rm GS}$ in the ground state (GS) rather than the square of the dipole itself $\langle\hat{\mu}^2\rangle_{\rm GS}$. In this work, we do not employ the coherent state representation, but we still expect the DSE to contain the physics of the ground state problem, to leading order. Though, our approach goes well-beyond the mean-field approach, incorporating, in principle, the exact electron-photon correlation by direct diagonalization in the adiabatic-Fock representation. In this case (Fig. 8), it is clear that the DSE is directly related to the chemically relevant modifications to the ground state energies (to a first approximation), since the DSE contribution nearly quantitatively reproduces the changes to the TS barrier energy in all cases (*i.e.*, other contributions largely cancel among each other). This also provides confirmation of the various mean-field QED-HF calculations[5,13,15,16,20,21,31] as well as high-level approaches[4,8,9,13,14,17,18,32–37] in the community exploring ground state cavity-modifications.[10,12,23–26]

Conclusions

We have shown that coupling a textbook ground state DA reaction to an quantized cavity photon allows for strong isomer selectivity, which is not observed outside the cavity under standard reaction conditions. Our results show that the cavity induces selectivity toward the endo isomer, even for moderate coupling strength as well as for random molecular orientations. In addition, we have shown that pQED-TDDFT method qualitatively agree with the high-level scQED-CCSD approach and with errors between the two approaches less than 3 kcal/mol, in agreement with reported errors between DFT and CCSD methodologies outside the cavity. This work, thus, provides an important and necessary benchmark with the high-level self-consistent QED coupled cluster approach which is commonly used to explore *ab initio* molecular polaritons.

By computing the ground state difference density, we show that the cavity induces a redistribution of electron density to stabilize or destabilize the TS geometry depending on the cavity polarization direction. Cavity-induced stabilization occurs by shifting electron density from intramolecular π-bonding orbitals to intermolecular bonding orbitals. Destabilization occurs through the opposite mechanism where the intermolecular bonding orbitals donate their electron density to intramolecular π-bonding orbitals. Thus, our results have provided a chemically relavent description of the cavity-induced changes to the ground state chemistry and thus changes to the molecular orbital theory inside the cavity.[21]

We extended this exploration to an arbitrary cavity polarization vector which leads to critical polarization angles that maximize the endo-/exo-selectivity of the reaction. Here, we show that the optimal selectivity for the ground state reaction, in terms of the cavity polarization direction, does not well-correspond to a simple chemically relavent direction but rather involves complicated interplay between the many permanent and transition dipole orientations of the reacting molecules. Overall, we show that maximum selectivity for the endo and exo isomers can be achieved with relative barrier energies approaching $\sim$5 and $\sim$10 k_BT, respectively. In the absense of orientational ordering, we find that the endo isomer is preferred by $\sim k_BT$ even in a collection of randomly oriented molecules coupled to the cavity.

Finally, we decompose the energy contributions from the Hamiltonian and provide a discussion on the effects of the dipole self-energy on the polaritonic ground state. The DSE contribution to the TS barrier energy has identical trends with the energy of the total Hamiltonian. Thus, we conclude that the DSE is the leading order physics to the cavity-mediated ground state modifications, which is in agreement with many other works at the mean-field QED-HF level and beyond. We hope this work enables further study of ground state chemistry inside the cavity that includes (i) identification of the optimal cavity polarization direction for each reaction (ii) a quantitative benchmark against other approaches, and (iii) a detailed comparison of the cavity parameters with state-of-the-art experimental cavity designs.

Acknowledgement This work was supported by the Air Force Office of Scientific Research under AFOSR Award No. FA9550-23-1-0438. During the early stage of this work, J.W. and B.M.W were partially supported by the National Science Foundation's "Center for Quantum Electrodynamics for Selective Transformations (QuEST)" under grant number CHE-2124398. P.H. appreciates the support of the Cottrell Scholar Award (a program by the Research Corporation for Science Advancement). Computing resources were provided by the Center for Integrated Research Computing (CIRC) at the University of Rochester.

Supporting Information Available

Additional figures that support the discussion in the main text are provided, namely, light-matter coupling strength scans, pQED-TDDFT/scQED-CCSD benchmark comparisons, three-dimensional isosurfaces of the difference density, and energy contributions of reactant and transition state geometries.

References

(1) Anslyn, E. V.; Dougherty, D. A. *Modern Physical Organic Chemistry*; University Science Books, 2006.

(2) Loudon, M.; Parise, J. *Organic Chemistry*; Macmillan Learning, 2015.

(3) Woodward, R. B.; Hoffmann, R. Stereochemistry of Electrocyclic Reactions. *J. Am. Chem. Soc.* **1965**, *87*, 395–397.

(4) Pavošević, F.; Smith, R. L.; Rubio, A. Computational study on the catalytic control of endo/exo Diels-Alder reactions by cavity quantum vacuum fluctuations. *Nat Commun* **2023**, *14*, 2766.

(5) Mandal, A.; Taylor, M. A. D.; Weight, B. M.; Koessler, E. R.; Li, X.; Huo, P. Theoretical Advances in Polariton Chemistry and Molecular Cavity Quantum Electrodynamics. **2023**, *123*, 9786–9879.

(6) Taylor, M. A. D.; Mandal, A.; Zhou, W.; Huo, P. Resolution of Gauge Ambiguities in Molecular Cavity Quantum Electrodynamics. *Phys. Rev. Lett.* **2020**, *125*, 123602.

(7) Mandal, A.; Taylor, M. A. D.; Huo, P. Theory for Cavity-Modified Ground-State Reactivities via Electron–Photon Interactions. *J. Phys. Chem. A* **2023**, *127*, 6830–6841.

(8) Pavošević, F.; Hammes-Schiffer, S.; Rubio, A.; Flick, J. Cavity-Modulated Proton Transfer Reactions. *J. Am. Chem. Soc.* **2022**, *144*, 4995–5002.

(9) Pavosevic, F.; Smith, R. L.; Rubio, A. Cavity Click Chemistry: Cavity-Catalyzed Azide-Alkyne Cycloaddition. 2023; `http://arxiv.org/abs/2305.09496`.

(10) Mandal, A.; Taylor, M. A. D.; Huo, P. Theory for Cavity-Modified Ground-State Reactivities via Electron–Photon Interactions. *J. Phys. Chem. A* **2023**, *127*, 6830–6841.

(11) Weight, B. M.; Krauss, T. D.; Huo, P. Investigating Molecular Exciton Polaritons Using Ab Initio Cavity Quantum Electrodynamics. *J. Phys. Chem. Lett.* **2023**, *14*, 5901–5913.

(12) Haugland, T. S.; Philbin, J. P.; Ghosh, T. K.; Chen, M.; Koch, H.; Narang, P. Understanding the polaritonic ground state in cavity quantum electrodynamics. 2023; `http://arxiv.org/abs/2307.14822`.

(13) Haugland, T. S.; Ronca, E.; Kjønstad, E. F.; Rubio, A.; Koch, H. Coupled Cluster Theory for Molecular Polaritons: Changing Ground and Excited States. *Phys. Rev. X* **2020**, *10*, 041043.

(14) Haugland, T. S.; Schäfer, C.; Ronca, E.; Rubio, A.; Koch, H. Intermolecular interactions in optical cavities: An ab initio QED study. *J. Chem. Phys.* **2021**, *154*, 094113.

(15) Foley, J. J., IV; McTague, J. F.; DePrince, A. E., III Ab initio methods for polariton chemistry. *Chemical Physics Reviews* **2023**, *4*, 041301.

(16) Weight, B. M.; Li, X.; Zhang, Y. Theory and modeling of light-matter interactions in chemistry: current and future. *Phys. Chem. Chem. Phys.* **2023**,

(17) DePrince, A. E. Cavity-modulated ionization potentials and electron affinities from quantum electrodynamics coupled-cluster theory. *J. Chem. Phys.* **2022**, *154*, 094112.

(18) DePrince, A. E. Cavity-modulated ionization potentials and electron affinities from quantum electrodynamics coupled-cluster theory. *J. Phys. Chem. A 2022, 126, 49, 9303–9312* **2022**, *154*, 094112.

(19) Weight, B.; Weix, D.; Tonzetich, Z.; Krauss, T.; Huo, P. Cavity Quantum Electrodynamics Enables para- and ortho-Bromination of Nitrobenzene. *ChemRxiv https://doi.org/10.26434/chemrxiv-2023-l0lwk* **2023**,

(20) Li, X.; Zhang, Y. First-principles molecular quantum electrodynamics theory at all coupling strengths. 2023; `http://arxiv.org/abs/2310.18228`.

(21) Riso, R. R.; Haugland, T. S.; Ronca, E.; Koch, H. Molecular orbital theory in cavity QED environments. *Nat. Commun.* **2022**, *13*, 1368.

(22) Akselrod, G. M.; Huang, J.; Hoang, T. B.; Bowen, P. T.; Su, L.; Smith, D. R.; Mikkelsen, M. H. Large-Area Metasurface Perfect Absorbers from Visible to Near-Infrared. *Advanced Materials* **2015**, *27*, 8028–8034.

(23) Flick, J.; Schäfer, C.; Ruggenthaler, M.; Appel, H.; Rubio, A. Ab Initio Optimized Effective Potentials for Real Molecules in Optical Cavities: Photon Contributions to the Molecular Ground State. *ACS Photonics* **2018**, *5*, 992–1005.

(24) Rokaj, V.; Welakuh, D. M.; Ruggenthaler, M.; Rubio, A. Light–matter interaction in the long-wavelength limit: no ground-state without dipole self-energy. *J. Phys. B: At. Mol. Opt. Phys.* **2018**, *51*, 034005.

(25) Schäfer, C.; Ruggenthaler, M.; Rokaj, V.; Rubio, A. Relevance of the Quadratic Diamagnetic and Self-Polarization Terms in Cavity Quantum Electrodynamics. *ACS Photonics* **2020**, *7*, 975–990.

(26) Ruggenthaler, M.; Flick, J.; Pellegrini, C.; Appel, H.; Tokatly, I. V.; Rubio, A. Quantum-electrodynamical density-functional theory: Bridging quantum optics and electronic-structure theory. *Phys. Rev. A* **2014**, *90*, 012508.

(27) Jaynes, E. T.; Cummings, F. W. Comparison of quantum and semiclassical radiation theories with application to the beam maser. *Proc. IEEE* **1963**, *51*, 89–109.

(28) Epifanovsky, E. et al. Software for the frontiers of quantum chemistry: An overview of developments in the Q-Chem 5 package. *J. Chem. Phys.* **2021**, *155*, 084801.

(29) Chikkaraddy, R.; de Nijs, B.; Benz, F.; Barrow, S. J.; Scherman, O. A.; Rosta, E.; Demetriadou, A.; Fox, P.; Hess, O.; Baumberg, J. J. Single-molecule strong coupling at room temperature in plasmonic nanocavities. *Nature* **2016**, *535*, 127–130.

(30) Philbin, T. G. Generalized coherent states. *Amer. J. Phys.* **2014**, *82*, 742–748.

(31) Schnappinger, T.; Sidler, D.; Ruggenthaler, M.; Rubio, A.; Kowalewski, M. Cavity Born–Oppenheimer Hartree–Fock Ansatz: Light–Matter Properties of Strongly Coupled Molecular Ensembles. *J. Phys. Chem. Lett.* **2023**, *14*, 8024–8033.

(32) Weight, B. M.; Tretiak, S.; Zhang, Y. Diffusion quantum Monte Carlo approach to the polaritonic ground state. *Phys. Rev. A* **2024**, *109*, 032804.

(33) Vu, N.; McLeod, G. M.; Hanson, K.; DePrince, A. E. Enhanced Diastereocontrol via Strong Light–Matter Interactions in an Optical Cavity. *J. Phys. Chem. A* **2022**, *126*, 9303–9312.

(34) Yang, J.; Ou, Q.; Pei, Z.; Wang, H.; Weng, B.; Shuai, Z.; Mullen, K.; Shao, Y. Quantum-electrodynamical time-dependent density functional theory within Gaussian atomic basis. *J. Chem. Phys.* **2021**, *155*, 064107.

(35) Yang, J.; Pei, Z.; Leon, E. C.; Wickizer, C.; Weng, B.; Mao, Y.; Ou, Q.; Shao, Y. Cavity quantum-electrodynamical time-dependent density functional theory within Gaussian atomic basis. II. Analytic energy gradient. *The Journal of Chemical Physics* **2022**, *156*, 124104.

(36) McTague, J.; Foley, J. J. Non-Hermitian cavity quantum electrodynamics–configuration interaction singles approach for polaritonic structure with ab initio molecular Hamiltonians. *J. Chem. Phys.* **2022**, *156*, 154103.

(37) Pavošević, F.; Flick, J. Polaritonic Unitary Coupled Cluster for Quantum Computations. *J. Phys. Chem. Lett.* **2021**, *12*, 9100–9107.

TOC Graphic